Fatigue crack inspection and characterisation using non-collinear shear wave mixing

Authors and Addresses:

Hongtao Lv[a,b], Jie Zhang[b], Jingpin Jiao[a] and Anthony Croxford[b]

[a] Department of Mechanical Engineering and Applied Electronics Technology, Beijing University of Technology, West Dawang Road, Beijing 100124, China

[b] Department of Mechanical Engineering, University of Bristol, University Walk, Bristol, BS8 1TR, UK

Keywords:

Non-collinear shear wave mixing, nonlinear ultrasonics, fatigue crack, crack sizing

ABSTRACT

In recent years, nonlinear ultrasonic techniques have been developed rapidly for defect detection and characterization at its early development stage. In this paper, non-collinear shear wave mixing is used for fatigue crack detection and characterization, exploring how orientation and size may be determined. This is achieved through measuring the amplitude of the generated longitudinal wave from a crack of interest. This amplitude is a function of the interaction angle and frequency ratio of two incident shear waves and the resulting amplitude parameter space is termed the nonlinear fingerprint of the crack. Numerical analysis of the nonlinear interaction between two incident shear waves and cracks was performed using two-dimensional finite element models to explore a broader parameter space than possible experimentally. It is shown that the interaction angle which leads to the maximum generated longitudinal wave amplitude is related to the orientation angle of the crack. To confirm these conclusions the model was validated using experimental measurements of vertical fatigue cracks grown using 3-point bending tests from initiation notches. The polarity flipping method was used to improve signal to noise ratio in such measurements. It is shown that there is a good agreement between the experimentally measured fingerprints and those simulated using finite element methods. Finally, an approximate method for sizing fatigue cracks was introduced that uses multiple non-collinear measurements along the crack length to determine its extent. As expected, the measured sizes from the proposed method indicate greater crack lengths than seen with linear ultrasonic phased array images due to the closed fatigue cracks being undetectable with linear arrays.

1 INTRODUCTION

Fatigue cracks are a common defect type which can lead to structural failure in a range of important industrial sectors such as aerospace, nuclear, transportation and petrochemical [1]. Early stage fatigue cracks are typically difficult to detect with conventional linear ultrasonic techniques, being tightly closed and with low acoustic contrast. If detection of closed fatigue cracks were more reliable it could provide early warning of damage, in turn allowing better scheduling of maintenance and/or the timely implementation of measures to extend material life.

Due to their significant promise to improve the detectability of the defects at early development stage, nonlinear ultrasonic techniques have been developed rapidly in recent years [1-5]. These techniques rely on material or defect nonlinearity modulating incident ultrasonic signals and moving energy to new frequencies creating new ultrasonic signals, e.g., subharmonic frequency [6-7], second or higher harmonic frequencies [8-10], shifted resonant frequency [11-12] and the combinations of frequencies of incident waves [13-22]. These new outputs resulting from nonlinear interactions are generally known as nonlinear signals. In practical inspections, nonlinear signals are also generated by the experimental equipment itself such as transducers, coupling media and amplifiers, making it difficult to determine the origin of nonlinearity and reliably detect damage. This is one of the main barriers to using the subharmonic or higher harmonic nonlinear signals to inspect structures [13, 14]. This problem can be mitigated to some extent by using non-collinear wave mixing methods in which the nonlinear signals arising from material and defect interaction can be separated from those associated with experimental elements through the selection of wave mode, frequency and spatial location [13, 14].

In the non-collinear wave mixing method, the interaction between two incident ultrasonic signals, can lead to the generation of nonlinear signals with a frequency equal to the sum or difference of the incident waves [23-26]. There are two main sources of these nonlinear signals. One is the material nonlinearity in a solid, which can result from plastic ageing [15], oxidative ageing [16] and plastic deformation [17, 18] and is mathematically related to the material third order elastic constants under the existence of a strain energy function [23-26]. The other is contact acoustic nonlinearity (CAN) resulting from the contact dynamics of two surfaces in features such as kissing bonds [19-22] and fatigue cracks [27-30]. Under high acoustic stress condition, these surfaces will be alternately opening, closing and slipping. This distorts the harmonic acoustic waves and leads to the generation of nonlinear signals.

Jones and Kobett [23], Taylor and Rollins [24], Zarembo and Krasil'Nikov [25] investigated the physical mechanism of resonant wave generation in the interaction of two incident elastic waves in isotropic solids, termed as the classical nonlinear theory of wave mixing. They found that there are several combinations of incident waves that can lead to the generation of a resonant wave. Korneev

and Demčenko [26] summarized the analytical solutions and relevant resonant conditions for all possible nonlinear interactions of ultrasonic waves. Based on this theoretical understanding, the nonlinear wave mixing techniques have been used for detection and evaluation of different material damages in their early development stage. For example, Tang et al. [17] used primary shear and longitudinal waves to localize plastic deformation. Sun et al. [18] applied the non-collinear wave mixing technique to localize plastic zones and assess plastic strain. Croxford et al. [13] used the non-collinear shear-wave mixing technique to assess plasticity and fatigue damage.

There is a smaller body of work investigating non-collinear mixing with CAN. Zhang et al. [31] developed analytical and 2D finite element (FE) models to predict the additional nonlinearity caused by the interaction between imperfect interfaces and non-collinear shear waves. Blanloeuil et al. [32] built a 2D FE model to investigate the interaction between two shear waves and closed cracks. They showed that the non-collinear wave mixing technique could be used for the detection and characterization of closed cracks. This work showed that the interaction between contacting defect surfaces and two incident shear waves can lead to the generation of longitudinal waves scattered in different directions to those resulting from classical wave mixing in materials.

Recently, Alston et al. [22] measured experimentally the amplitudes of the nonlinear signals generated from the interaction between two non-collinear incident shear waves and horizontal interfaces. These amplitudes were shown as a function of the interaction angle and the frequency ratio of two incident shear waves and the resulting parameter space was termed the fingerprint of the interface. It was found that the interaction angle leading to maximum nonlinear signals from a horizontal interface is around 80° far from the 120° predicted from the material nonlinearity measured using the classical resonant wave mixing method. This means that the resonant conditions required for measuring material nonlinearity [18, 22] may not be the same as for CAN [22, 32, 33] from an interface. The further investigation of this on real fatigue cracks is a primary motivation of this paper. Specifically, can the approach of measuring the parameter space of the non-collinear shear wave mixing technique be used to detect and characterize fatigue cracks?

To explore this a 2D FE model is first introduced in section 2 and was used to simulate the fingerprint of cracks at a variety of orientation angles from the non-collinear shear wave mixing measurements.

This essentially enables a greater range of parameters to be investigated than is possible experimentally. The experimental system used to validate this model is shown in section 3. Simulated fingerprints from the FE model are shown and analysed in section 4. These are then compared to experimental measurements from vertical fatigue cracks for validation in section 5. In section 6, the effect of instrument and transducer dynamics on the experimental measurements were discussed. Finally, an approach to fatigue crack sizing using the experimental measurements is proposed.

2 MODEL

Before introducing the numerical model that will be used throughout a light background on classical wave mixing will be introduced. This is important for aiding the interpretation of later experimental results which will show both material and CAN nonlinearity.

2.1 Classical wave mixing theory

According to the classical wave mixing theory, the interaction of two primary incident waves can generate a new wave. This wave has a frequency equal to either the sum or the difference of the two primary waves and is formed under the resonant condition expressed mathematically as [23, 24],

$$f_g = f_1 \pm f_2, \tag{1}$$

$$\mathbf{k}_g = \mathbf{k}_1 \pm \mathbf{k}_2, \tag{2}$$

where f is the frequency of a wave, $\mathbf{k}$ is the wave vector and $|\mathbf{k}| = k = 2\pi f/v$, v is the phase velocity of the wave, the subscript 1, 2, g represent the first, second primary incident waves and the new generated resonant wave respectively. The geometric representation of equation 2 is illustrated in Figure 1. Also shown in Figure 1 is the interaction angle of two incident waves, α, and the scattering angle of the new generated wave relative to $\mathbf{k}_1$, φ. Using the law of cosines, α and φ can be calculated from [26],

$$\left(\frac{f_g}{v_g}\right)^2 = \left(\frac{f_1}{v_1}\right)^2 + \left(\frac{f_2}{v_2}\right)^2 \pm 2\frac{f_1}{v_1}\frac{f_2}{v_2}\cos\alpha, \tag{3}$$

$$\tan\varphi = \frac{\pm\frac{v_1}{v_2} r\sin\alpha}{1\pm\frac{v_1}{v_2} r\cos\alpha}, \tag{4}$$

where $r = f_2/f_1$ is the frequency ratio of two incident waves.

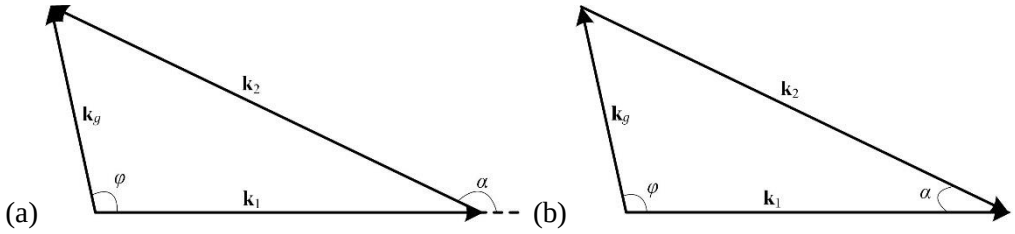

Figure. 1 Geometric representation of two incident waves mixing to generate a resonant wave at the resonant condition with a case of; (a) sum-frequency (b) difference-frequency.

It is noted that, due to $-1 \leq \cos\alpha \leq 1$ and wave polarization restrictions, there are only ten possible incident wave combinations which satisfy the resonant conditions and can generate a resonant wave [26]. In practice, the use of the interaction of two incident shear waves to generate a longitudinal wave with the sum frequency is a commonly used configuration [13] due to its experimental simplicity. The resonant conditions for this case are as shown in Figure 2 and can be calculated using equations 3-4. Here, the material properties from aluminium were used and they include the longitudinal velocity of 6374 m/s, shear wave velocity of 3160 m/s and Poisson's ratio of 0.33. To satisfy the resonant condition, the interaction angle α is at least 120° while the frequency ratio *r* must be between 0.34 and 2.94.

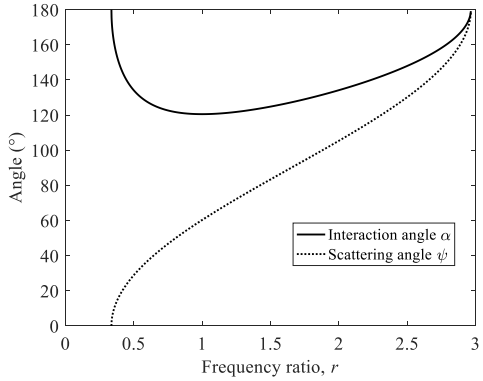

Figure. 2 Theoretical classical resonant conditions of the interaction angle and the scattering angle from the interaction of two incident shear waves.

2.2 Finite element model used to understand the generation of nonlinear signals from the interaction between two incident shear waves and a crack

In this paper, a 2D time domain FE model is used to investigate the generation of nonlinear signals from a non-collinear shear wave mixing measurement on a crack. The model was built and operated

in Abaqus Explicit 6.14 (Dassault Systems Simulia Corp. Johnston, RI, USA) and its geometry is shown in Figure 3. The main parts in the model are a pair of ultrasonic sources, T_1 and T_2, located symmetrically relative to the model centre line on a semicircle boundary, a modelled crack and a number of monitoring nodes on a flat bottom boundary used to record displacements. Note that the source surfaces are modelled as straight chords to ensure the generation of plane waves. This approach allows the interaction angle α to be set through the central locations of the sources and keeps the wave propagation distance between the sources and the crack center unchanged in all wave interaction angle cases, ensuring that same input amplitude is applied to the crack in all cases. The incident ultrasonic waves are generated through displacements at the nodes on the source surfaces. These displacements are the sinusoidal signals with a frequency of f_1 and f_2 for T_1 and T_2 respectively with the specific excitation described in Section 4. The directions of the displacements control the wave mode of the incident waves. For example, displacement perpendicular to the straight source surfaces leads to longitudinal waves while tangential to the surfaces generates shear waves. The crack is represented as an ellipse with a length of l on the long axes, an orientation angle of γ relative to the lateral direction and it is modelled by removing the elements within the crack boundary. The crack surface is split as two symmetrical surfaces along its length direction which were set as a master and a slave surface under hard contact condition with a defined friction coefficient. The nonlinear signals of interest were extracted from the recorded displacements on the monitor nodes in post-processing. The geometry, size of input transducer and receivers, is set up to recreate that used experimentally later to aid comparison.

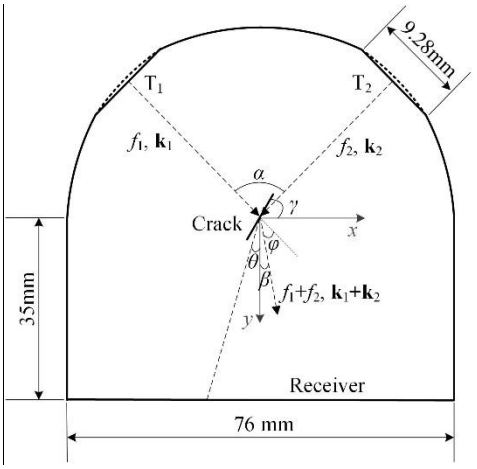

Figure. 3 The structure of a 2D finite element model used to investigate the nonlinear signals from a non-collinear shear wave mixing measurement on a crack.

In the process, the time windows are first set according to the theoretical travelling time from the crack center to the monitor nodes and then used to extract the raw-signals of interest from the recorded displacements. These raw-signals are then processed to extract the frequencies of interest using a bandpass frequency filter with a central frequency of $f_g = f_1 + f_2$. The amplitudes of these signals are finally extracted using the Hilbert transform to give the amplitudes of the nonlinear signals. However, when the frequency ratio is close to one, this frequency filter is not able to isolate the nonlinear signal of interest at $f_g = f_1 + f_2$ from that generated at second harmonic frequency ($2f_1$ or $2f_2$). Instead, when operating close to a frequency ratio of 1, three FE models with the same mesh but different source excitation conditions were used to extract the nonlinear signals of interest properly. In these FE models, the first model has the source excited only at T_1, the second one has the source excited only at T_2 and the third one has the sources excited at both T_1 and T_2. The nonlinear signals of interest were extracted by the subtraction of the monitored displacements from the third model and the summation of those from the first two models to suppress the $2f_1$ or $2f_2$ terms. However, the computation cost of such simulation is expensive and it was only used for the cases of the frequency ratio ranging from 0.9 to 1. For the other cases, one FE model combined with a suitable frequency filter was used to simulate one amplitude in the fingerprint.

In the FE model, linear plane strain triangle element CPE3 was used and the maximum size of the element is less than one tenth of the minimum wavelength of the two incident shear waves and the generated longitudinal wave from the crack nonlinearity. In order to only monitor the nonlinearity

from cracks and get rid of the nonlinearity induced from other sources, in the FE models, third order elastic constants were not used in material properties and there is hence no material nonlinearity. The nonlinear effects of large displacements were also disabled (Nlgeom is off in Abaqus).

It is noted that each FE model run can only produce a result for a specific crack interacting with incident waves at a specific combination of frequency ratio and interaction angle. Each FE model run can hence generate only one nonlinear amplitude in the fingerprint of the crack. The nonlinear signals from a specific interaction angle but different frequency ratios can be generated from the FE models with the same mesh but different frequency displacements loaded on the sources. In order to generate ultrasonic waves consistent with those seen experimentally in each FE model, the surface at each source location was cut to a flat surface in the tangential direction of the arch at its middle point.

Finally, to aid the comparison of simulation and experimental results, there are two angles defined in Figure 3, i.e., θ and β. θ is the angle of the straight line from the crack centre to a monitor node relative to y direction. β is the theoretical steering angle of the nonlinear signal at the classical resonant condition relative to y direction and $\beta = \alpha/2 - \varphi$.

3 EXPERIMENTAL MEASUREMENT SYSTEM AND METHOD

Before comparing the numerical and experimental results the experimental system will be introduced.

3.1 Experimental measurement system and specimens

Figure 4 shows the experimental system used for measuring the nonlinear signals from cracks using the non-collinear shear wave mixing technique. In this system, two signals were generated initially from two Agilent 33250A arbitrary waveform generators (manufactured by Agilent, Santa Clara, USA). These signals are then amplified by a 75A250A and 100A400 (manufactured by Amplifier Research, USA) respectively, and transmitted by two 5MHz centre frequency Panametrics transducers, T_1 and T_2, to generate two longitudinal ultrasonic waves. These transducers were installed in a frame immersed in a water tank. The incident angles and the lateral separation distance of these transducers were controlled by motors in the frame. The two generated longitudinal ultrasonic waves first propagate into water and then mode convert to shear waves when transmitted into the

specimen of interest. The interaction angle of the converted shear waves and the interaction location were controlled by the incident angles, the lateral separation distance and a pre-set stand off distance of the transducers, with these parameters calculated using Snell's law [34]. A 128 element, 0.25mm pitch, 10MHz ultrasonic array probe made by Imasonic was placed on the bottom surface of the specimen and a Micropulse FMC array controller (manufactured by Peak NDT, UK) was used to receive the signals. A thermal circulator SVT-SVPR-BAG (manufactured by PolyScience, USA) was used to keep temperature of water at a constant 25ºC to reduce the effect of temperature on the nonlinear signal generation. The whole measurement is controlled by a program written using Matlab (MathWorks, USA).

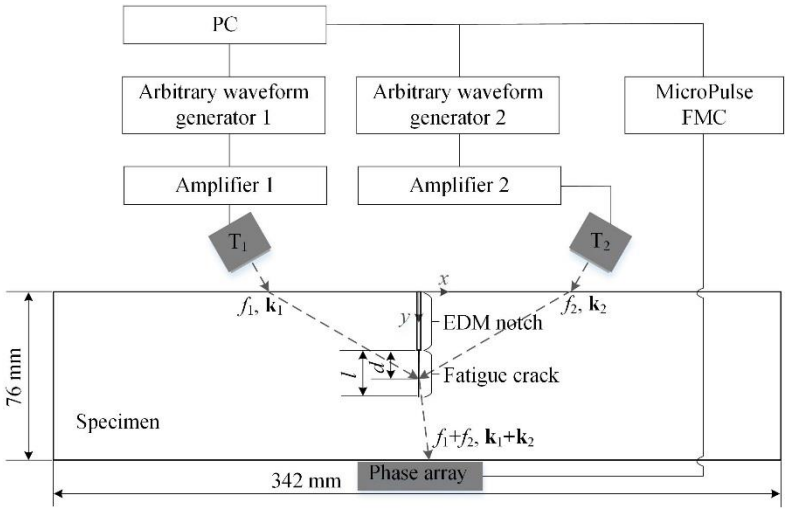

Figure. 4 Schematic diagram of the experimental system used to measure the nonlinear signals from cracks using the non-collinear shear wave mixing technique.

In a measurement, the ultrasonic transducers (made by Olympus, USA) have an active aperture size of 10 mm, a measured central frequency of 4.7 MHz and a bandwidth of 3.4 MHz at the threshold of -6 dB of the peak amplitude. Two 20-cycle Hann-windowed tone-burst signals with the same amplitude but different central frequencies and initial phases were generated by the signal generators. The initial phases were set to make sure that the two waves can arrive at the centre of the interaction area at the same time. The central frequency of transducer T_1 was fixed at 5 MHz while that of T_2 was varied from 2 MHz to 7 MHz to vary the frequency ratio from r = 0.4 to 1.4. The separation distance and the inclination angles of the two transducers were controlled in the range of 40 mm to 160 mm and 0° to 25° relative to the sample thickness direction to achieve the measurements with an interaction angle

ranging from 80° to 130° and the interaction location ranging from 12 mm to 38 mm below the top surface of a specimen. The gain of each amplifier was set as 55 dB. The array probe aperture allowed 38.35 mm on the bottom surface of a specimen to be monitored with measurements focused on reception.

The experimental measurements were conducted on a number of aluminum specimens 342 mm×76 mm×31.5 mm with different features. An initial EDM notch was cut from the middle with a length of 22.5 mm and a width of 0.1 mm. A vertical fatigue crack was then grown from this notch through 3-point bending using an Instron 8872 hydraulic test machine. The load on the test machine was sinusoidally varied with a frequency of 6 Hz, a minimum force of 1 kN and maximum force of 18 kN. Fatigue cracks with sizes ranging from 1 mm to 13 mm (at the surface) were fabricated using different numbers of load cycles. Note that the experimental measurements were only performed on vertical cracks due to the difficulties of making real cracks with other orientation angles. As shown in Figure 4, the crack length is defined as l, the wave interaction location can be defined by either y relative to the top surface of a specimen or d relative to the EDM notch tip. $d < 0$ indicates that the interaction area is above the notch tip while $d > 0$ that it is below the notch tip. In the experimental measurements, the crack lengths were measured using both the TFM image-based method [35, 36] and the proposed nonlinear technique and they are defined as l_{m1} and l_{m2} respectively. Note that l_{m1} is measured as the distance in the image from the end of the EDM starter notch to the farthest crack tip.

3.2 Polarity flipping method

In this paper, the polarity flipping method [20] was used to improve SNR in the experimental measurements. This method can suppress not only incoherent noise but also coherent 'noise' from the fundamental waves and harmonic waves of two incident shear waves though the superposition of the responses from four input signals with same amplitude and frequency but different initial phases.

The details of the method are described in here. An elastic structure with a defect can be considered as a quadratic system described by,

$$y(t) = \alpha x(t) + \beta x^2(t), \tag{5}$$

where $x(t)$ is an input signal, $y(t)$ is the output signal and α, β are constants. Two transducers, T_1 and T_2, are used to load four input signal pairs on the structure. In these input signals, the amplitude and frequency from T_1 is fixed as A_1 and f_1 respectively while those from T_2 is A_2 and f_2, however, the initial phase varies. This leads to four sequential input fields as [20],

$$f^{++}(t) = A_1 \sin(2\pi f_1 t) + A_2 \sin(2\pi f_2 t), \tag{6}$$

$$f^{\mp}(t) = A_1 \sin(2\pi f_1 t + \pi) + A_2 \sin(2\pi f_2 t), \tag{7}$$

$$f^{\pm}(t) = A_1 \sin(2\pi f_1 t) + A_2 \sin(2\pi f_2 t + \pi), \tag{8}$$

$$f^{--}(t) = A_1 \sin(2\pi f_1 t + \pi) + A_2 \sin(2\pi f_2 t + \pi), \tag{9}$$

Combined Equations (5)-(9), the sequential output signals can be expressed as,

$$g^{++}(t) = \alpha A_1 \sin(2\pi f_1 t) + \alpha A_2 \sin(2\pi f_2 t) - \beta \frac{A_1^2}{2} \cos[2\pi(2f_1)t] - \beta \frac{A_2^2}{2} \cos[2\pi(2f_2)t] + \beta A_1 A_2 \cos[2\pi(f_2 - f_1)t] - \beta A_1 A_2 \cos[2\pi(f_2 + f_1)t] \tag{10}$$

$$g^{\mp}(t) = \alpha A_1 \sin(2\pi f_1 t + \pi) + \alpha A_2 \sin(2\pi f_2 t) - \beta \frac{A_1^2}{2} \cos[2\pi(2f_1)t + 2\pi] - \beta \frac{A_2^2}{2} \cos[2\pi(2f_2)t] + \beta A_1 A_2 \cos[2\pi(f_2 - f_1)t - \pi] - \beta A_1 A_2 \cos[2\pi(f_2 + f_1)t + \pi] \tag{11}$$

$$g^{\pm}(t) = \alpha A_1 \sin(2\pi f_1 t) + \alpha A_2 \sin(2\pi f_2 t + \pi) - \beta \frac{A_1^2}{2} \cos[2\pi(2f_1)t] - \beta \frac{A_2^2}{2} \cos[2\pi(2f_2)t + 2\pi] + \beta A_1 A_2 \cos[2\pi(f_2 - f_1)t + \pi] - \beta A_1 A_2 \cos[2\pi(f_2 + f_1)t - \pi] \tag{12}$$

$$g^{--}(t) = \alpha A_1 \sin(2\pi f_1 t + \pi) + \alpha A_2 \sin(2\pi f_2 t + \pi) - \beta \frac{A_1^2}{2} \cos[2\pi(2f_1)t + 2\pi] - \beta \frac{A_2^2}{2} \cos[2\pi(2f_2)t + 2\pi] + \beta A_1 A_2 \cos[2\pi(f_2 - f_1)t] - \beta A_1 A_2 \cos[2\pi(f_2 + f_1)t + 2\pi] \tag{13}$$

The final averaged signal can be then written as [20],

$$g(t) = \frac{g^{++}(t) - g^{\mp}(t) - g^{\pm}(t) + g^{--}(t)}{4} = \beta A_1 A_2 \cos[2\pi(f_2 - f_1)t] - \beta A_1 A_2 \cos[2\pi(f_2 + f_1)t] \tag{14}$$

In this way, the final signal $g(t)$ only contains the signals with sum and difference frequencies of the input signals [20]. The sum-frequency longitudinal wave can be then extracted using a band-pass filter

with a center frequency of $f_1 + f_2$. It is noted that the process of using $g(t)$ at various interaction angles and frequency ratios to obtain the experimentally measured fingerprints from material and a defect is the same as that used in the simulation described in section 2.2 enabling comparison.

4 SIMULATION RESULTS OBTAINED USING FE MODELS

As described the FE model was designed to model the effect of shear-shear interaction with contacting surfaces. The model was specifically designed to recreate the conditions seen experimentally. This is seen in Figure 3, where the diameter of the upper semi-circular boundary is 76 mm and the vertical distance between the crack centre and the bottom boundary of the model is 35 mm, the same geometry and positions seen in the experimental measurements. This ensures the nature of the wave fronts at the interaction point and the measurement locations are consistent between model and experiment, eliminating them as variables. Displacements with an amplitude of 20 nm were loaded along the tangential direction of the arch of each source surface to generate two incident shear waves. These were 20 cycle Hann-windowed sinusoidal signals and each source surface has an aperture size of 9.28 mm. The long and short axes of the modelled ellipse-shape crack are 5 mm and 20 nm respectively. The friction coefficient of the modelled hard contact crack surfaces is 0.3 [32]. It is noted that the friction coefficient was selected with reference to [32] and includes both clapping and slipping effect from crack surfaces. The material is modelled as aluminium with a density of 2700 kg/m^3, a Young's modulus of 69 GPa and a Poisson ratio of 0.33. The maximum element size is 20 μm. It took 4 hours to run each model on a standard computer with 8GB memory. In order to compare with the experimental measurements easily, the monitored displacements along the *y* axis direction, essentially the same as measurements made with the phased array, were used to generate the fingerprints.

To generate a fingerprint of a crack of interest, multiple FE models are required to run. In these FE models, the locations of the sources were changed to achieve the interaction angle varying from α = 60° to 130° with an increment of 5°. The central frequency of the source T_1 is fixed as f_1 = 5 MHz while that of T_2 ranges from f_2 = 3 MHz to 7 MHz with increments of 0.5 MHz leading to the frequency ratio varying from r = 0.6 to 1.4 with an increment of 0.1. The orientation angles of the

cracks are varied as γ = 0° (horizontal), 30°, 60° and 90° (vertical). The bandwidth of the frequency filters used to extract filtered-signals was fixed at 1 MHz of the interaction frequency.

4.1 Fingerprints from cracks with various orientation angles

Figure 5(a) shows the filtered interaction signal obtained from the horizontal crack (γ = 0°) at the monitoring node at x = 2.13mm. This corresponds to a scattered angle of the nonlinear signal of $\theta = \beta$ = 3.48º and was recorded with α = 80° and a frequency ratio of r = 0.9. The first arrival signal packet in Figure 5(a) is the filtered-signal of interest. Figure 5 (b) shows the extracted peak amplitudes of the envelopes of the filtered-signals of interest from all monitoring nodes in the FE models with the horizontal crack, an interaction angle of α = 80° and various frequency ratios. Note that the peak amplitude of the envelope of the first arrival signal packet in Figure 5(a) corresponds to the amplitude at (3.48º, 0.9) in Figure 5(b). Also shown in Figure 5 (b) is a white curve which indicates the steering angles β of the nonlinear signals calculated from the classical nonlinear theory (Equation 4). Comparing the white curve and the peak amplitudes in each row in Figure 5 (b), it can be seen that the classical nonlinear theory is doing a good job at predicting the steering angles of the nonlinear signals from a horizontal crack. Therefore, in the post-processing of the filtered-signals from the FE models, the peak amplitudes of the envelopes at the steering angles predicted from the classical nonlinear theory (equation 4) were used as the values in the simulated fingerprints.

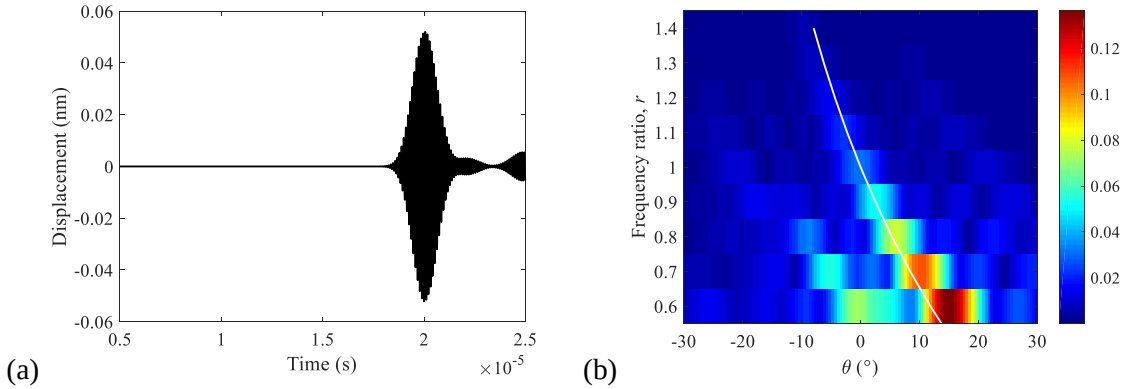

Figure. 5 Examples of FE simulation results from the horizontal crack (γ = 0º) with an interaction angle of α = 80° for; (a) a filtered signal at a frequency ratio of r = 0.9 and (b) peak amplitudes of all filtered signals at various frequency ratios. Note that the peak amplitude in (a) corresponds to the amplitude at (3.48, 0.9) in (b).

Figure 6(a) shows the modelled fingerprint from the horizontal crack (γ = 0°), essentially the nonlinear amplitude seen at a range of interaction angles and frequency ratios. From Figure 6(a) it can be seen that the amplitude of the nonlinear signal is greater at lower frequency ratios and that the overall peak is seen at an interaction angle of α = 90°. This is different to that expected for the nonlinear signals from material nonlinearity, i.e., α = 120° [18, 22]. The same FE model simulation procedure was repeated for the cracks with an orientation angle of γ = 30°, 60° and 90° (vertical). Again, in the simulated results, it is shown that the classical nonlinear theory can be used to predict the steering angles of the nonlinear signals from all modelled cracks. Here, the simulated fingerprints are shown in Figure 6(b-d) for cracks with an orientation angle of γ = 30°, 60° and 90° (vertical) respectively. Comparing Figures 6(a-d), it can be seen that amplitude is inversely proportional to frequency ratio at all interaction angles for all cracks. However, the interaction angles at which the maximum amplitude nonlinear response is seen varies in each case and is thus related to the crack orientation angle. These angles are also smaller than the theoretical interaction angle predicted from the classical nonlinear theory, shown in Figure 2. This means that the resonant condition defined in Equation 3 is, as expected not valid for the nonlinearity resulting from the contact dynamics of cracks.

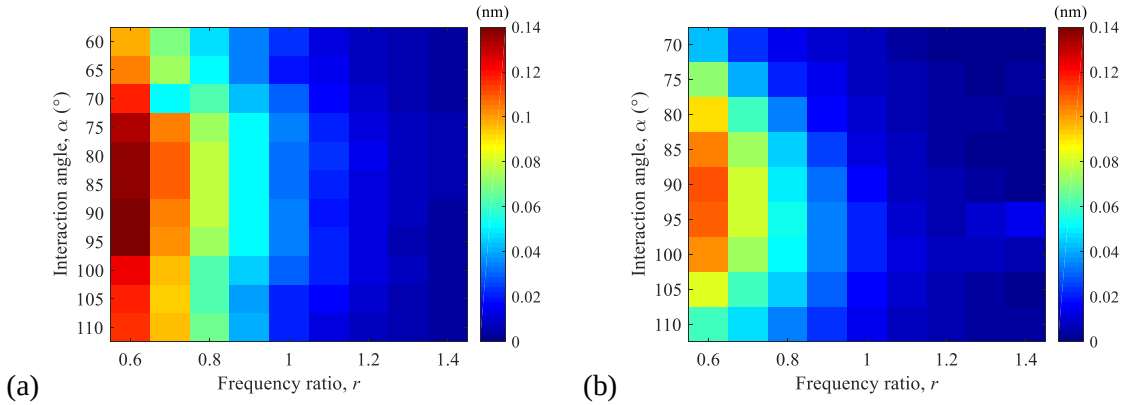

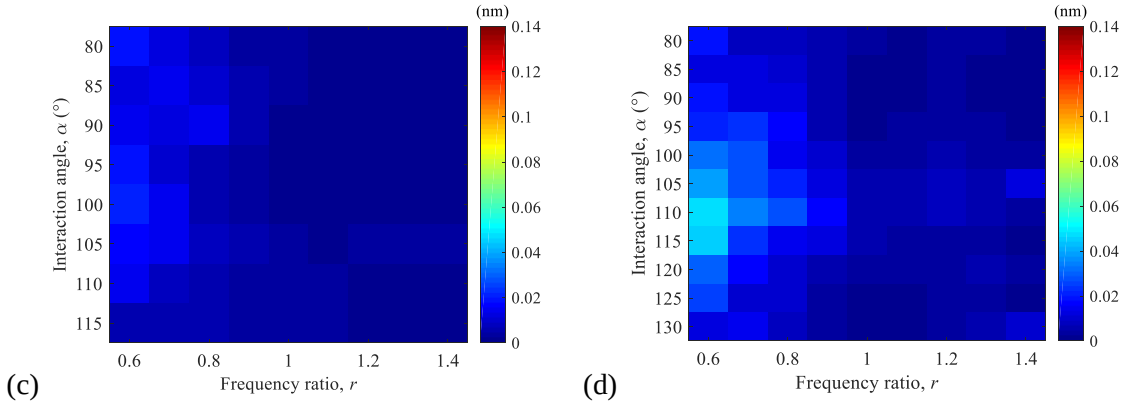

Figure. 6 The Fingerprints of the nonlinear signals from the crack with an orientation angle of; (a-d) 0º, 30º, 60º and 90º. Note that 0º and 90º correspond to horizontal and vertical cracks respectively.

It is noted that there is a good agreement between Figure 6(a) and the fingerprint shown in [22] and [32] for the kissing bond interfaces, particularly in the interaction angles leading to the largest nonlinear amplitude. Previous studies have shown that both clapping and slipping effects on the crack surfaces can contribute to the generation of the nonlinear signals [32, 37]. Comparing Figures 6(a-d) it is can be seen that the interaction angle leading to the maximum amplitude, α_p, for a specific crack angle at each frequency ratio is almost unchanged, so frequency ratio is relatively unimportant. This therefore suggests that all that is required to determine the dominant closed crack orientation is to measure the angle of interaction that leads to the peak response. As an example, Figure 7 shows these interaction angles, α_p, at the cracks with various orientation angles and this shows the potential to use α_p to measure crack orientation angle. A higher resolution simulation would be required to measure changes in interaction angle smaller than 5 degrees, however the concept has been clearly demonstrated here.

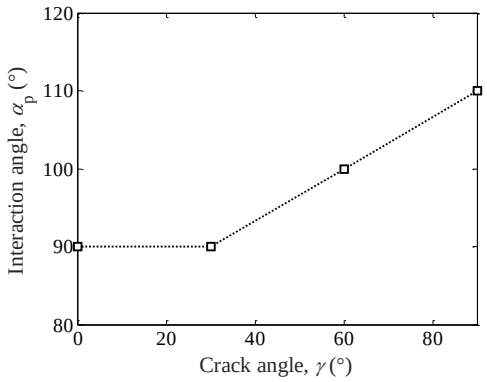

Figure. 7 The interaction angles at the maximum amplitude in each figure in Figure 6 when the frequency ratio is 0.8.

4.2 Nonlinearity amplitude from the vertical cracks with various lengths

Having shown that we can extract orientation from non-collinear measurements we will now investigate how such measurements may be used to size closed cracks. To explore this the case of a vertical crack was used (which can be experimentally validated) but the approach should be general to crack orientation. FE models were run with a vertical crack at a fixed location but with various lengths. The crack was inspected with two shear waves at an interaction angle of 110^o (where the peak response is observed) and a frequency ratio of 0.8. The procedure to extract the nonlinear amplitude from the displacements on the monitoring nodes was the same as that described in section 4.1. Figure 8 shows the simulated results as a function of crack length. It can be seen that the nonlinear amplitude increases gradually with crack length when it is less than 10 mm. Here the crack is smaller than the interaction area (roughly 10mm diameter but investigated in more detail later), so the amplitude of the nonlinear signal grows as the crack becomes a greater percentage of the whole until it bridges the entire interaction area. At this point the crack length is greater than 10 mm, and the nonlinear amplitude begins to converge as increases in crack length are outside the interaction area. We believe the small fluctuations in Figure 8 are caused by the numerical error in the FE simulation resulting from a different mesh being used to model each crack length. The sidelobes of the two incident waves could also cause amplitude fluctuation in large cracks. It is important to note that in reality the amplitude variation in the interaction region is continuous so it would not be expected to lead to a sharp cutoff. Figure 8 shows a solid curve used to fit all measured points with the least square method, this monotonically increases with crack length at the beginning and then converges. The location with the peak amplitude in this curve, i.e., l = 10 mm, should indicate the case when the crack is fully contained by the interaction region of the two incident shear waves. Thus by moving the interaction region along a crack and measuring the nonlinear amplitude its size could be measured.

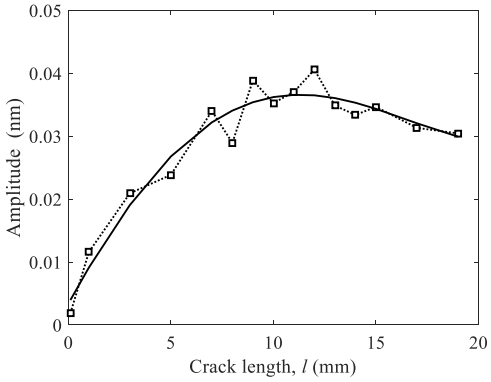

Figure. 8 Amplitude of the nonlinear signal as function of vertical crack length from FE models with an interaction angle of 110º and a frequency ratio of 0.8.

5 EXPERIMENTAL MEASUREMENTS

In this section, non-collinear shear wave mixing experiments were performed on vertical fatigue cracks in aluminium specimens to validate the corresponding FE simulation results. Such measurements have not been made with real vertical fatigue cracks, and are essential to give confidence in the conclusions reached from the numerical modelling. The repeatability of the experimental measurements was also demonstrated.

5.1 Experimentally measured fingerprints

In this section, the experimentally measured fingerprints from a plain reference specimen without starter notch or fatigue crack and one with EDM starter notch and a long fatigue crack are presented. In the measurements, the polarity flipping method described in section 3.2 was used to capture the nonlinear signals from the interaction area of interest. This was repeated over a range of interaction angle and frequency ratios. The maximum amplitude from each group of nonlinear signals at one combination of the interaction angle and frequency ratio was then extracted as a single value in the fingerprint. The final fingerprint results when all combinations of interaction angle and frequency ratio have been measured.

As an example, Figures 9(a-d) shows the experimentally measured raw-signals $g^{++}(t)$, $g^{\mp}(t)$, $g^{\pm}(t)$ and $g^{--}(t)$ respectively using the polarity flipping method with an interaction angle of 120º and a frequency ratio of 0.8. The interaction location is at y = 29 mm on a plain reference specimen without starter notch or fatigue crack. Figure 9(e) is the combination of Figures 9(a-d) using equation 14.

Comparing Figures 9(a-d) and Figure 9(e), it is clear that the SNR of the nonlinear signals is significantly improved using the polarity flipping method. The SNR can be further improved through the frequency filter process, as shown in Figure 9(f). It is noted that the maximum amplitude in Figure 9(f) is used as the value in the experimentally measured fingerprint at r = 0.8 and α = 120º.

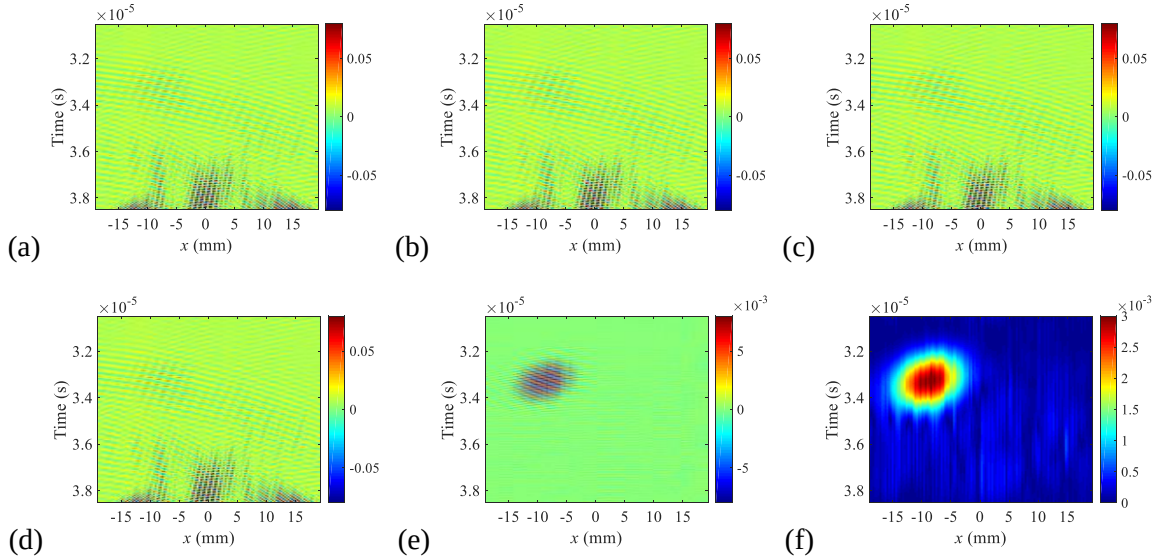

Figure. 9 The experimentally measured raw-signal of; (a) $g^{++}(t)$, (b) $g^{\mp}(t)$, (c) $g^{\pm}(t)$, (d) $g^{--}(t)$ and (e) $(g^{++} - g^{\mp} - g^{\pm} + g^{--})/4$. (f) is the envelope of (e) after filtering. These results were obtained using the polarity flipping method with an interaction angle of 120º and a frequency ratio of 0.8 with the wave interaction region at y = 20 mm on a plain reference specimen without starter notch or fatigue crack.

In contrast to numerical results, experimentally measured signals contain nonlinearity from both material (classical wave mixing nonlinearity) and possible defect (CAN) sources. The modelling work carried out suggests that the peak angle of interaction can be used as a feature to identify the origin of these measured effects. Figures 10(a-b) compare the experimentally measured fingerprint of a plain reference specimen without starter notch or fatigue crack and one with the EDM starter notch and a long fatigue crack (l_{m1} = 7.8 mm) at an interaction location of y = 29 mm (6.5mm below the end of the starter notch). In Figure 10(a), the reference specimen, the interaction angle at the peak nonlinear amplitude, α_p, is around 120º while α_p is around 110º in Figure 10(b), the fatigue cracked case. This shows a good agreement with the prediction from the classical nonlinear theory (Figure 2) and the FE models (Figure 6(d)). It is also shown that the amplitude from crack nonlinearity is around one-order magnitude higher that from material nonlinearity. Thus by recording the complete parameter space

rather than a single interaction angle or frequency ratio the origin of a nonlinear signal can be determined. This shows the potential of using the location of α_p and nonlinearity amplitude to detect cracks and their orientation.

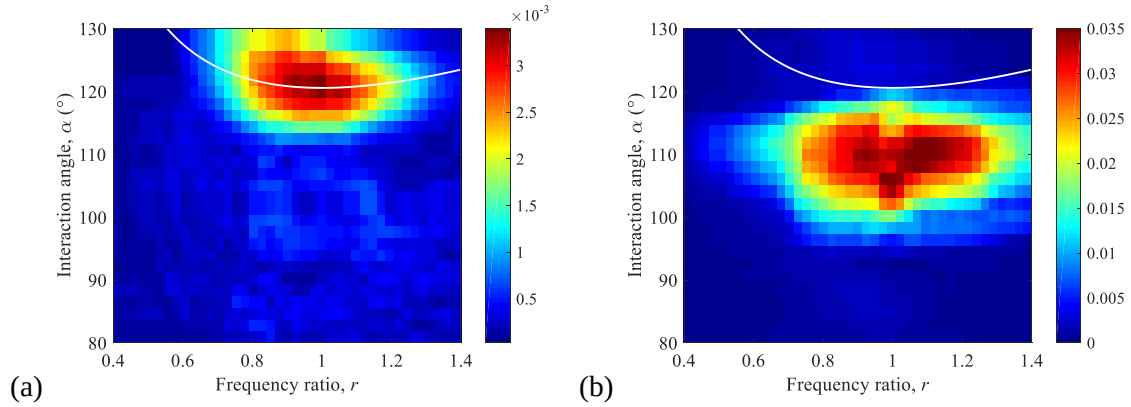

Figure. 10 The experimentally measured fingerprint at the interaction location of y = 29 from a specimen; (a) without any inside feature and (b) with a long crack (l_{m1} = 7.8 mm).

5.2 Repeatability of the measurements

To ensure that the measurement effect was genuine, repeatability tests were made on a range of samples with nominal crack lengths of l_{m1} = 7.8 mm, 8.3 mm and 8.3 mm with an interaction angle of 110°, a frequency ratio of 0.8 and scanned through interaction locations. The measurements were repeated three times on each specimen and the results are as shown in Figure 11. The repeatability of the measurements on each specimen is excellent and demonstrates the robustness of using the non-collinear shear wave mixing method to inspect fatigue cracks. Also shown in Figure 11 is that the amplitudes from the reference specimen (pink circles) remains broadly consistent at all interaction depths as the material nonlinearity remains largely consistent through depth. The amplitudes from the cracked specimens show self-consistent trends, an initial monotonic increase, a peak and then monotonic decrease. This is consistent with expectations, as the interaction area is moved down more of the crack will be activated. As the interaction area continues to move down so less of the crack is within it and the nonlinear amplitude drops off.

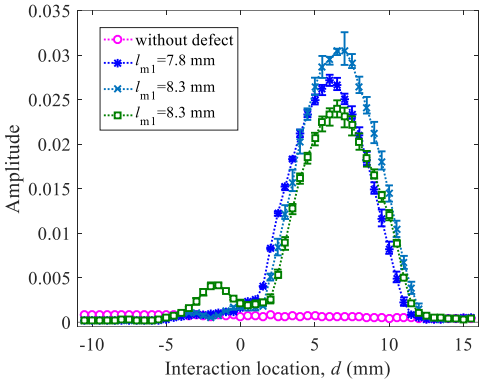

Figure. 11 The repeatability of the experimental measured nonlinear amplitudes from different specimens as a function of the interaction location d when interaction angle is 110º and frequency ratio is 0.8.

6 DISCUSSION

6.1 Energy of incident waves

Comparing Figure 6(d) and Figure 10(b), it can be seen that there is a good agreement in the interaction angle leading to largest amplitude, α_p, however not in the frequency ratio. As the model suggests the important parameter is interaction angle this is not so significant, however it is important to understand its origin. The numerical simulation takes no account of the finite bandwidth of real transducers, assuming perfect response at all frequencies. In addition, it does not account for changes in the amplitude in the part as a result of changes in transmission coefficient. In order to check these effects the transduction properties, bandwidth and transmission coefficients must be measured and used to correct the simulated responses.

In the experimental measurements, the central frequency of transducer T_1 was fixed at f_1 = 5 MHz. Therefore the energy conditions on the incident waves will only be affected by the transfer function of transducer T_2 and its connected amplifier and the phased array. It is noted that the former two are a function of $f_2 = rf_1$ and the phased array response can be considered as a function of $f_1 + f_2 = (1 + r)f_1$. Hence all these transfer functions can be considered as a function of the frequency ratio, r, at a fixed f_1. Here, the transfer functions of transducer T_2 and the phased array were measured from the square root of the 50 ns-wide rectangular pulse echo signal reflected from a water-solid interface. The

transfer function of the amplifier was measured as the ratios between the peak amplitudes of an input and the output sinusoidal signals at various frequencies. These measured transfer functions are shown in Figures 12(a-c). Figure 12(d) shows the theoretical transmission coefficient from a water-solid interface as a function of the interaction angle of two incident shear waves [34].

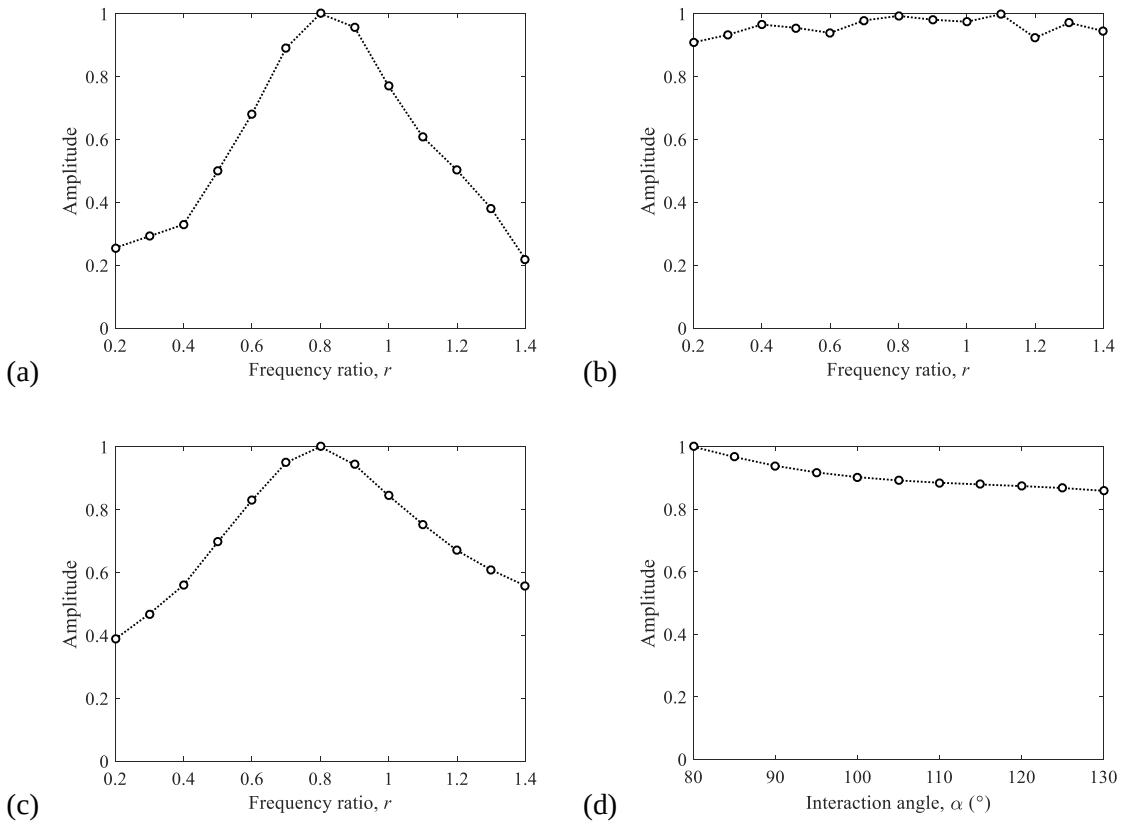

Figure. 12 The experimentally measured transfer function from; (a) transducer T_2, (b) amplifier connected with T_2 and (c) the phased array. (d) is the theoretically predicted transmission coefficient from the water-solid interface.

Assuming the amplitude from crack nonlinearity increases linearly with the increase of the amplitude of the incident waves, Figures 12(a-d) can be used to correct the simulated fingerprints to some extent. Figure 13(a) shows the multiplication of Figure 6(d) and Figures 12(a-d) at each corresponding interaction angle and frequency ratio. Comparing Figure 13(a) with Figure 6(d), it can be seen that the interaction angle leading to largest amplitude, α_p, keeps unchanged as 110° while the frequency ratio becomes larger. Compared with Figure 6(d), Figure 13(a) shows a better agreement with the experimentally measured fingerprint as shown in Figure 10(b). Figure 13(b) compares the nonlinear

amplitude as a function of interaction angle from the simulations and the experimental measurements on a vertical crack when the frequency ratio is 0.8. In Figure 13(b), one simulation curve, labelled as sim1, is from Figure 6(d) obtained from the FE models. The other simulation curve, labelled as sim2, is the multiplication of Figure 6(d) and Figures 12(d). Comparing three curves in Figure 13(b), it can be seen that there is a good agreement in α_p = 110° and the effect of the transfer functions of the phased array on α_p is negligible. Even without correcting the simulation results it is important to note that the interaction angle at which the crack effects take place remains unchanged.

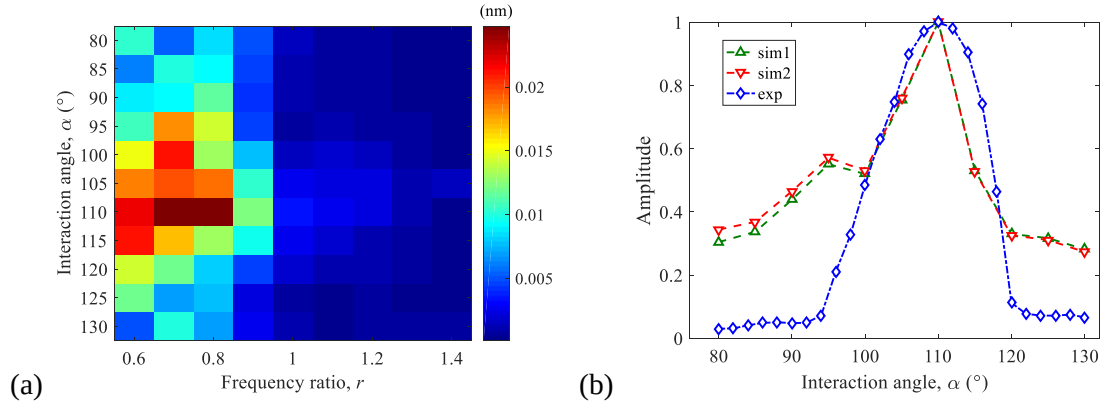

Figure. 13 (a) The corrected simulated fingerprint from the modelled vertical crack. It is the multiplication of Figure 6(d) and Figures 12(a-d). (b) The comparison of the nonlinear amplitude as a function of interaction angle from the simulations and the experimental measurements on a vertical crack when frequency ratio is 0.8.

6.2 Size of wave interaction area

The result from section 4.2 suggests that the amplitude of the nonlinear response peaks when a crack is activated entirely within the area of interaction. For the case presented in section 4.2 this equated to a characteristic size of 10mm. This is however entirely dependent on the beam profiles at any point. Before the nonlinear response can be used for sizing it is important to understand the extent of the interaction area. Here, Huygens principle was used to simulate the acoustic pressure fields from the inspection configurations used in the FE models (as shown in Figure 3) and the experimental measurements (as shown in Figure 4) and they are as shown in Figure 14 (a) and 14 (b) respectively. Both configurations have two incident shear waves with an interaction angle of 110º and a frequency ratio of 0.8, however only the experimental configuration includes the water coupling layer and it is

this that results in the slightly different beam profiles. The amplitude in each figure is normalized to its own maximum and displayed on a dB scale.

As mentioned in section 4.2, the maximum nonlinear amplitude in Figure 8 occurs when the crack is fully activated by the two incident shear waves. This means the crack length at the maximum amplitude, i.e. l = 10 mm, is equal to the size of the intersection area of the two incident shear waves. From Figure 14(a) it can be calculated that the amplitude threshold is -6.5 dB when the width of the intersection area along the thickness direction is a = 10 mm. This threshold can be considered as a conservative threshold to define the interaction area. Using this amplitude threshold, Figure 14 (c) shows the width of the interaction area for the experimental configuration with an interaction angle of 110º, a frequency ratio of 0.8 and with varying interaction depth. As expected, the width of the intersection area increases as the interaction area moves further from the top surface due to beam spreading.

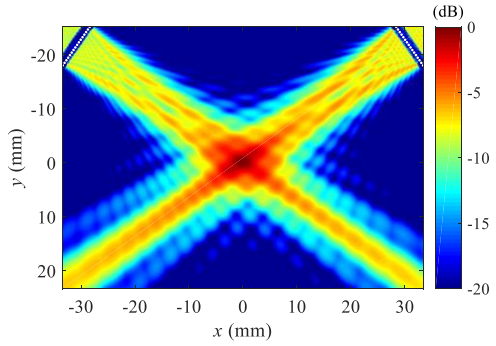

(a)

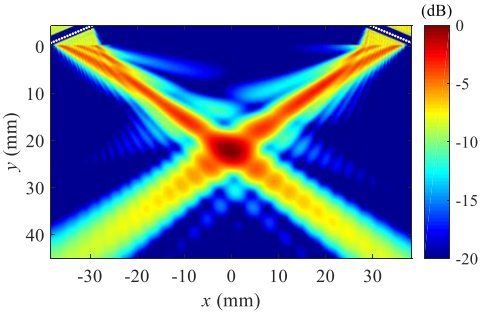

(b)

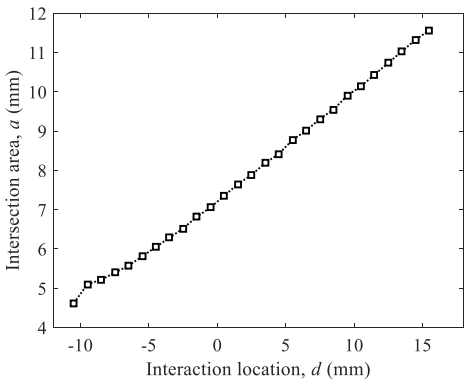

(c)

Figure. 14 The simulated acoustic pressure distribution at an interaction location of y = 23 mm in a configuration used in; (a) the FE simulations and (b) the experimental measurements. (c) is the width of the intersection area of two incident waves in the experimental configuration as a function of the interaction location d. Note that both configurations have two incident shear waves with an interaction angle of 110º and a frequency ratio of 0.8.

6.3 Sizing fatigue cracks

With knowledge of the interaction area the crack may now be approximately sized. Figure 15(a) shows a few examples of the experimentally measured nonlinear amplitudes from a range of vertical fatigue cracks as a function of interaction location, d, when the interaction angle is 110° and the frequency ratio is 0.8. In Figure 15(a), the interaction location with the peak amplitude, d_p, should correspond to the case when the closed part of the crack tip aligns with the highest amplitude area in the incident waves, while the interaction location with a convergent amplitude close to zero after the peak, d_e, should correspond to the case when the high energy area of the incident waves is away from the crack tip. Using the amplitude at d = -10 mm as the amplitude threshold for extracting d_e, Figure 15(b) compares the measured crack size using the TFM image-based method, l_{m1}, with d_p, d_e from a group of predominantly vertical fatigue cracks. As shown in Figure 15(b), in all measurements of crack length, d_e is the largest and l_{m1} is greater than d_p. This is because the crack tips are partially closed hence have some visibility in the TFM images and can also lead to the nonlinear signals. The end of the crack tips should be between d_p and d_e. Conservatively, the measured crack length can be d_e,i.e. extend out until the nonlinear amplitude has returned to the background level. Less conservatively, we can assume that the peak nonlinear amplitude happens when a partially closed crack is fully activated within the effective incident wave interaction area, as analysed in section 4.2 and 6.2, the measured crack length can therefore be defined as,

$$l_{m2} = d_p + a/2, \tag{15}$$

where, a is obtained from Figure 14(c). This metric assumes that though the peak indication comes from location d_p the crack will extend at the peak across the entire interaction area. Comparing l_{m1} and l_{m2} in Figure 15(b) it can be seen that the measured crack lengths using the non-collinear shear wave

mixing method are 2-3 mm longer than those using the TFM image-based sizing method. The difference is due to the closure condition of the fatigue cracks making their linear detection impossible and the incident wave energy distribution around the cracks.

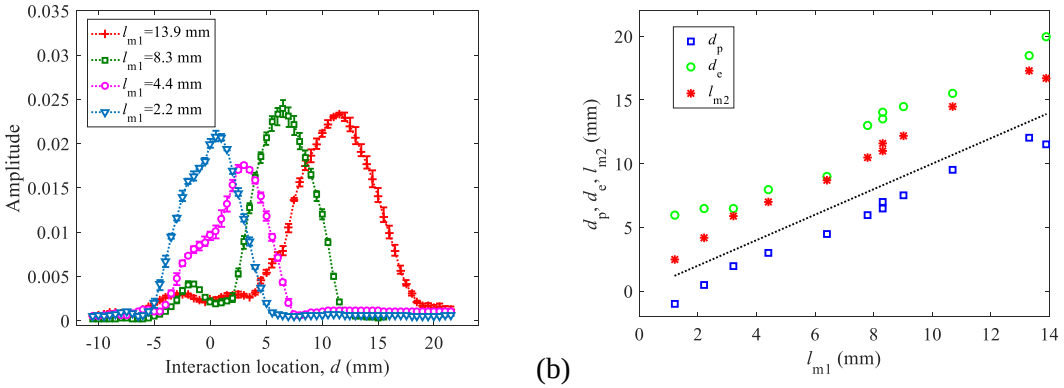

Figure. 15 (a) The examples of the amplitudes of the experimentally measured nonlinear signals as a function of the interaction location from the fatigue cracks with various lengths when the interaction angle is 110º and frequency ratio is 0.8. (b) The comparison of l_{m1}, d_p, d_e and l_{m2} measured from the fatigue cracks with various sizes. Note that l_{m1} was measured using the TFM image-based method and the others were obtained using the non-collinear shear wave mixing method. Note that the dotted line is the reference line with a unit gradient for comparing the measured crack lengths.

7 CONCLUSION

In this paper, the non-collinear shear wave mixing technology was used to inspect and characterise real fatigue cracks. 2D FE models were used to calculate the nonlinear amplitude fingerprints from the interaction between two incident shear waves and cracks with different orientation angles. These showed that the interaction angles leading to the peak nonlinear amplitude correlate well with crack orientation angle. Most usefully for characterisation these interaction angles indicative of CAN are different to that from material nonlinearity, i.e., 120°. This could be used to distinguish between material nonlinearity and that from cracks and shows the potential to measure the orientation angle of a crack. It is also shown that the classical nonlinear theory can be used to predict the steering angles of the nonlinear signals from cracks. In addition to characterizing the crack orientation, the simulation suggested that non-collinear shear wave measurements could also be used to size them.

The experimental measurements were performed on a number of real vertical fatigue cracks grown using 3-point bending tests. It is shown that there is a good agreement between the simulated and experimentally measured results on the location of the interaction angles leading to the largest nonlinear amplitude from the vertical cracks. This supported the conclusions of the modelling results. The effects of the transfer functions of the transducers, the amplifiers and the phased arrays on experimental measurements were analysed and used to correct simulated fingerprint of the vertical crack. This leads to the improved agreement in the fingerprints from simulation and experimental measurements. It is found that the measured nonlinear amplitude is the convolution of crack length and the size of the interaction region of the incident wave and this can be used to measure crack length. Measured crack lengths using the proposed method are around 2~3 mm greater than those measured using the conventional TFM image-based sizing technique. This could be caused by the partially closure of the cracks and the incident wave energy distribution around the cracks. However it is important to note that this sensitivity is also a function of how tightly closed the crack is.

The validated FE model could subsequently be used to explore the impact of peak interaction angle of more complex crack geometries. Cracks in real parts are typically complex and are unlikely to have a single peak at a specific angle. The FE model could be used to explore the impact that such a geometry may have on the indicated nonlinear response.

ACKNOWLEDGEMENTS

This work was supported by the National Key Research and Development Program of China (Grant No. 2016YFF0203002), National Natural Foundation of China (Grant No. 11572010, 11572011), and China Scholarship Council (Grant No. 201706540035). This work was also supported through the core research programme within the UK Research Centre in NDE (RCNDE) funded by EPRSC EPS (Grant No. EP/L022125/1).

REFERENCES

[1]. K. Y. Jhang, "Nonlinear ultrasonic techniques for nondestructive assessment of micro damage in material: a review", International journal of precision engineering and manufacturing, 10(1) 123-135 (2009)

[2]. D. Broda, W. J. Staszewski, A. Martowicz, T. Uhl and V. V. Silberschmidt, "Modelling of nonlinear crack–wave interactions for damage detection based on ultrasound—A review", Journal of Sound and Vibration, 333(4), 1097-1118 (2014)

[3]. U. Andreaus, P. Baragatti, P. Casini and D. Lacoviello, "Experimental damage evaluation of open and fatigue cracks of multi‐cracked beams by using wavelet transform of static response via image analysis", Structural Control and Health Monitoring, 24(4), e1902 (2017)

[4]. C. Zhou, M. Hong, Z. Q. Su, Q. Wang and L. Cheng, "Evaluation of fatigue cracks using nonlinearities of acousto-ultrasonic waves acquired by an active sensor network", Smart materials and structures, 22(1), 015018 (2012)

[5]. D. M. Joglekar and M. Mitra, "Time domain analysis of nonlinear frequency mixing in a slender beam for localizing a breathing crack", Smart Materials and Structures, 26(2), 025009 (2016)

[6]. D. Ginzburg, F. Ciampa, G. Scarselli and M. Meo. “SHM of single lap adhesive joints using subharmonic frequencies”, Smart Materials and Structures, 26(10), 105018 (2017)

[7]. M. Y. Zhang, L. Xiao, W. Z. Qu and Y. Lu, "Damage detection of fatigue cracks under nonlinear boundary condition using subharmonic resonance", Ultrasonics, 77, 152-159 (2017)

[8]. P. B. Nagy, "Fatigue damage assessment by nonlinear ultrasonic materials characterization", Ultrasonics, 36(1-5), 375-381 (1998)

[9]. K. Wang, Z. Fan and Z. Q. Su, “Orienting fatigue cracks using contact acoustic nonlinearity in scattered plate waves”, Smart Materials and Structures, 27(9), 09LT01 (2018)

[10]. C. Pruell, J. Y. Kim, J. M. Qu and L. J. Jacobs, “Evaluation of fatigue damage using nonlinear guided waves”, Smart Materials and Structures, 18(3),035003 (2009)

[11]. M. Muller, A. Sutin, R. Guyer, M. Talmant, P. Laugier and P. A. Johnson, "Nonlinear resonant ultrasound spectroscopy (NRUS) applied to damage assessment in bone", The Journal of the Acoustical Society of America, 118(6), 3946-3952 (2005)

[12]. A. Novak, M. Bentahar, V. Tournat, R. Guerjouma and L. Simon, "Nonlinear acoustic characterization of micro-damaged materials through higher harmonic resonance analysis ", NDT & E International, 45(1), 1-8 (2012)

[13]. A. J. Croxford, P. D. Wilcox, B. W. Drinkwater and P. B. Nagy, "The use of non-collinear mixing for nonlinear ultrasonic detection of plasticity and fatigue", The Journal of the Acoustical Society of America, 126(5), EL117-EL122 (2009)

[14]. A. Demčenko, R. Akkerman, P. B. Nagy and R. Loendersloot, "Non-collinear wave mixing for non-linear ultrasonic detection of physical ageing in PVC", NDT & E International, 49, 34-39 (2012)

[15]. A. Demčenko, V. Koissin and V. A. Korneev, "Noncollinear wave mixing for measurement of dynamic processes in polymers: Physical ageing in thermoplastics and epoxy cure", Ultrasonics 54(2), 684-693 (2014)

[16]. M. E. McGovern, W. G. Buttlar and H. Reis, "Characterisation of oxidative ageing in asphalt concrete using a non-collinear ultrasonic wave mixing approach", Insight-Non-Destructive Testing and Condition Monitoring, 56(7), 367-374 (2014)

[17]. G. X. Tang, M. H. Liu, L. J. Jacobs and J. M. Qu, "Detecting localized plastic strain by a scanning collinear wave mixing method", Journal of Nondestructive Evaluation, 33(2), 196-204 (2014)

[18]. M. X. Sun, Y. X. Xiang, M. X. Deng, J. C. Xu and F. Z. Xuan, "Scanning non-collinear wave mixing for nonlinear ultrasonic detection and localization of plasticity", NDT & E International, 93, 1-6 (2018)

[19]. E. Escobar-Ruiz, A. Ruiz, W. Hassan, D. Wright, L. Collison, P. Cawley and P. Nagy, "Non-linear ultrasonic NDE of titanium diffusion bonds", Journal of Nondestructive Evaluation, 33(2), 187-195 (2014)

[20]. Z. Y. Zhang, P. B. Nagy and W. Hassan, "Enhanced nonlinear inspection of diffusion bonded interfaces using reflected non-collinear ultrasonic wave mixing", AIP Conference Proceedings, 1706(1), 020023 (2016)

[21]. J. M. Qu, T. Ju, J. Achenbach and L. Jacobs. "A non-collinear mixing technique to measure the acoustic nonlinearity parameter of an adhesive bond from one side of the sample", The Journal of the Acoustical Society of America, 141(5), 3905-3905 (2017)

[22]. J. Alston, A. Croxford, J. Potter and P. Blanloeuil, "Nonlinear non-collinear ultrasonic detection and characterisation of kissing bonds", NDT & E International, 99, 105-116 (2018)

[23]. G. J. Jones and D. R. Kobett, "Interaction of elastic waves in an isotropic solid", The Journal of the Acoustical society of America, 35(1), 5-10 (1963)

[24]. L. H. Taylor and F. R. Rollins Jr, "Ultrasonic study of three-phonon interactions. I. Theory", Physical Review, 136(3A), A591 (1964)

[25]. L. K. Zarembo and V. A. Krasil'Nikov, "Nonlinear phenomena in the propagation of elastic waves in solids", Soviet Physics Uspekhi, 13(6), 778 (1971)

[26]. V. A. Korneev and A. Demčenko, "Possible second-order nonlinear interactions of plane waves in an elastic solid", The Journal of the Acoustical Society of America, 135(2), 591-598 (2014)

[27]. D. Donskoy, A. Sutin and A. Ekimov, "Nonlinear acoustic interaction on contact interfaces and its use for nondestructive testing", NDT&E International, 34(4), 231-238 (2001)

[28]. P. M. Thanseer, A. Kr. Metya, and S. P. Sagar, "Development of a non-collinear nonlinear ultrasonic-based technique for the assessment of crack tip deformation", Journal of Materials Engineering and Performance, 26(6) 2632-2639 (2017)

[29]. J. P. Jiao, H. T. Lv, C. F. He and B. Wu, "Fatigue crack evaluation using the non-collinear wave mixing technique", Smart Materials and Structures, 26(6), 065005 (2017)

[30]. H. T. Lv, J. P. Jiao, B. Wu and C. F. He, "Evaluation of fatigue crack orientation using non-collinear shear wave mixing method", Journal of Nondestructive Evaluation, 37(4), 74 (2018)

[31]. Z. Y. Zhang, P. B. Nagy and W. Hassan, "Analytical and numerical modelling of non-collinear shear wave mixing at an imperfect interface ", Ultrasonics, 65, 165-176 (2016)

[32]. P. Blanloeuil, A. Meziane and C. Bacon, "2D finite element modeling of the non-collinear mixing method for detection and characterization of closed cracks", NDT & E International, 76, 43-51 (2015)

[33]. A. Demčenko, L. Mainini, V. Korneev, "A study of the noncollinear ultrasonic-wave-mixing technique under imperfect resonance conditions", Ultrasonics, 57, 179 –89 (2015)

[34]. J. L. Rose, "Ultrasonic waves in solid media", Cambridge University Press, 57-61 (2004)

[35]. J. Zhang, B. W. Drinkwater and P. D. Wilcox, "The use of ultrasonic arrays to characterize crack-like defects", Journal of Nondestructive Evaluation, 29(4), 222-232 (2010)

[36]. C. Y. Peng, L. Bai, J. Zhang and B. W. Drinkwater, "The sizing of small surface-breaking fatigue cracks using ultrasonic arrays", NDT & E International, 99, 64-71 (2018)

[37]. P. Blanloeuil, A. Meziane and C. Bacon, "Numerical study of nonlinear interaction between a crack and elastic waves under an oblique incidence", Wave Motion, 51(3), 425-437 (2014)